Journal of Materials Chemistry C

Accepted Manuscript

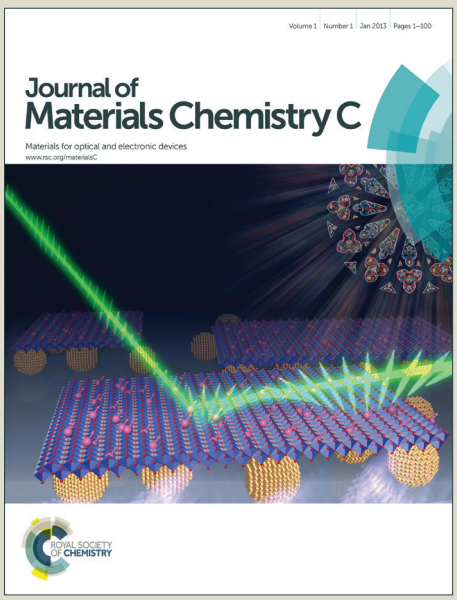

ROYAL SOCIETY OF CHEMISTRY

www.rsc.org/materialsC

Journal of Materials Chemistry C

Dynamic Article Links ►

Cite this: DOI: 10.1039/c0xx00000x

www.rsc.org/MaterialsC

Paper

Piezoelectric properties of individual nanocrystallites of $Ba_{0.85}Ca_{0.15}Zr_{0.1}Ti_{0.9}O_3$ obtained by Oxalate precursor route.

P.Bharathi[a], P.Thomas[b] and K.B.R.Varma[a*]

Received (in XXX, XXX) Xth XXXXXXXXX 20XX, Accepted Xth XXXXXXXXX 20XX

DOI: 10.1039/b000000x

Nanocrystalline $Ba_{0.85}Ca_{0.15}Zr_{0.1}Ti_{0.9}O_3$ (BCZT) powder was synthesized via the complex oxalate precursor route at a relatively low temperature (800°C/5h). The phase formation temperature of BCZT at nanoscale was confirmed by thermogravimetric (TG), differential thermal analysis (DTA) followed by X-ray powder diffraction (XRD) studies. Fourier Transform Infrared (FTIR) spectroscopy was carried out to confirm the complete decomposition of oxalate precursor into BCZT phase. The XRD and profile fitting revealed the coexistence of cubic and tetragonal phases and was corroborated by Raman study. Transmission electron microscopy (TEM) carried out on 800°C and 1000°C/5h heat treated BCZT powder revealed the crystallite size to be in the range of 20 – 50 nm and 40 – 200 nm respectively. The optical band gap for BCZT nanocrystalline powder was obtained using Kubelka Munk function and was found to be around 3.12 ± 0.02 eV and 3.03± 0.02 eV respectively for 800°C (20 – 50 nm) and 1000°C/5h (40 – 200 nm) heat treated samples. The piezoelectric properties were studied for two different crystallite sizes (30 and 70 nm) using piezoresponse force microscope (PFM). The d_{33} coefficients obtained for 30 nm and 70 nm sized crystallites were 4 pm/V and 47 pm/V respectively. These were superior to that of $BaTiO_3$ nanocrystal (≈ 50 nm) and promising from the technological/industrial applications view point.

Introduction

Lately, piezoelectric materials based nanostructures have attracted much attention for applications in nanoelectromechanical systems (NEMS) where they serve as nanogenerators that could convert mechanical vibrations into electricity to power nanoscale devices without batteries.[1-8] Several lead based materials have been in use so far. But due to environmental issues like recycling and disposal of lead in electronic products and its toxicity, lead based piezoelectric materials are banned worldwide.[9] Therefore, the researchers around the globe have been focusing on lead free materials with physical properties akin to that of lead zirconate titanate (PZT). Amongst different lead-free materials, Barium Calcium Zirconium Titanate (BCZT) is known to be promising piezo-ceramic possessing piezoelectric coefficient (d_{33}) in the range of 550 – 620 pC/N.[10] However, these were known to be synthesis route and microstructure dependent.

Synthesizing high purity materials and fabricating ceramics with the desired microstructure are some of the great challenges in the field of electro-ceramics. BCZT ceramics that were reported to possess promising piezoelectric properties were fabricated using the powders prepared by conventional solid-state reaction route. These powders were ball milled for longer durations (more than 12h) followed by calcinations at higher temperatures (typically around 1100-1300°C) with repeated grinding and sintering the green compacted powders at elevated temperatures. Dense ceramics were also fabricated using templated grain growth, hot pressing, besides microwave sintering.[11-13] The ceramics fabricated by these routes exhibited different piezoelectric properties which were ascribed to the presence of compositional heterogeneity. In order to address to the above issues and to achieve chemical homogeneity, we made an attempt to synthesize BCZT nanocrystalline powder at a reasonably low temperature for shorter duration via oxalate precursor route. The present method minimized several steps that are generally involved in synthesizing starting polycrystalline powdered samples before subjecting these to the sintering process using conventional methods. A number of reports are available in the literature[14-16] describing the synthesis of $BaTiO_3$ based materials through oxalate method and thermal decomposition of titanyl oxalates.[17] Recently calcium copper titanate (CCTO) nanocrystalline powder synthesized from oxalate precursor route was reported to have exhibited gaint dielectric constant close to 40,000 (1kHz) at room temperature.[18] This drew the attention of many researchers working in the field of electroceramics to see whether similar method could be used to synthesize BCZT at nanoscale. The objective of the present work was to explore the possibility of

[a]*Materials Research Centre, Indian Institute of Science, Bangalore-560012, India.*

[b]*Dielectric Materials Division, Central Power Research Institute, Bangalore-560080, Karnataka, India*

**E-mail: kbrvarma@mrc.iisc.ernet.in; Fax: +91 80 2360 0683; Tel: +91 080 2293 2914*

† Electronic supplementary information (ESI) available. See DOI:

synthesizing nanocrystalline powder and to visualize its piezoelectric properties. The BCZT ceramics fabricated using these powders associated with large grain sizes of 30μm exhibited piezoelectric coefficients (d_{33}) as high as 563 pC/N.[19] In this communication, the piezoelectric characteristics of 30 nm and 70 nm sized crystallites of BCZT are reported.

Experimental methods

Preparation of Barium calcium zirconyl titanyl precursor complex

The flowchart indicating the key steps that are involved in the synthesis of the nanocrystalline Barium Calcium Zirconium Titanate (BCZT) powder are summarized in Fig. 1.

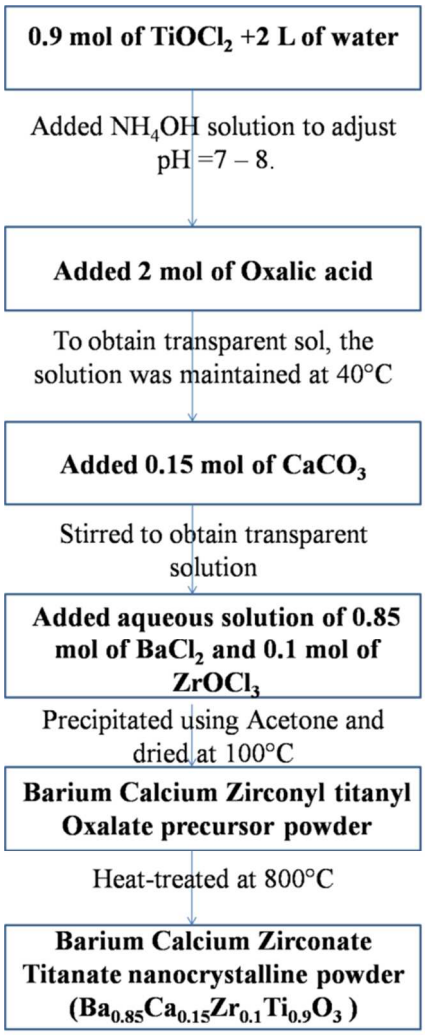

Fig.1 Flow-chart for the synthesis of BCZT nanopowder through oxalate precursor route.

The phase pure fine nanocrystalline powder of BCZT was obtained by controlled reaction between various precursors such as $TiOCl_2$ (obtained from $TiCl_4$ [Merck Germany]), Calcium carbonate (BDH; A.R. Grade), Barium chloride (Merck Germany; A.R Grade), Zirconyl oxy chloride (Nice, India; A.R. Grade), oxalic acid (S.D. Fine chemicals, analytical grade) and acetone (Emparta ACS. acetone for analysis ≥99.5 %). To begin with titania sol was prepared by adding NH_4OH (aqueous at 25°C) to the aqueous $TiOCl_2$ till the pH reached ~7.0 – 8.0. Subsequently, this sol was washed with distilled water for several times to ensure that the filtrate was free from NH_4Cl as confirmed by silver nitrate test. The obtained sol was mixed with 2 mols of oxalic acid and kept warm at 40°C to obtain a clear transparent solution. Thus obtained transparent sol was mixed with 0.15 mol of calcium carbonate and stirred continuously to evade any precipitate formation. Further, this solution was mixed with aqueous solution containing salts of barium chloride and zirconyl oxychloride. Then the final product of barium calcium zirconyl titanyl oxalate precursor complex (BCZT-OX) was precipitated out by adding acetone to the above solution. Finally, the thick precipitate that was obtained was washed several times using acetone and dried in air at room temperature (RT). The dried powder was subjected to thermal analyses to ascertain the calcination temperature that is required to obtain the desired monophasic barium calcium zirconium titanate.

Characterization

Thermal analyses were carried out using combined thermo gravimetric and differential thermal analyses (TG-DTA) (commercial TA instruments) in the temperature range of RT – 900°C at a heating rate of 10°C/min in flowing air ambience. Infrared (IR) spectra were recorded using a Perkin-Elmer FTIR spectrophotometer employing KBr disc technique. The monophasic nature of the final calcined powder was confirmed by X-ray powder diffraction technique (Pananalytical, X-Pert Pro) in the 2θ range of 20° - 70°. The grain size and its morphology were investigated using transmission (JEOL JEM-2001F) electron microscopes. The diffuse reflectance spectra for BCZT nanocrystalline powder were recorded using UV-Vis spectrophotometer (Perkin-Elmer Lambda 750) associated with 60mm (RSA ASSY) integrating sphere. Micro-Raman measurements were done at room temperature in the range of 50 – 1000 cm^{-1} using Raman spectrometer (WITec Alpha 300) with a spectral resolution of 3 cm^{-1} in 180° backscattering geometry for the as-prepared precursor complex powder and the samples heat treated at 800°C and 1000°C/5h. A frequency doubled Nd:YAG laser of excitation radiation 532 nm (in continuous mode) was used for this purpose. The excitation power on the surface of sample was maintained at a minimum value (~20 mW) to avoid any damage caused by the focused laser beam. Piezo Force Microscope (PFM) technique (Dimension Icon AFM, Bruker AXS GmbH, Karlsruh, Germany) was adopted to study the piezoresponse and local polarization switching behavior of the BCZT nanocrystallite. BCZT nanocrystalline powder was dispersed in ethanol and spin coated on platinum coated Si substrate and was found to be structurally homogenous. In order to make the powder adhere to the substrate, a small amount of Polyvinylpyrrolidone (PVP) binder was used. PFM was operated in vertical mode with an AC driving voltage of $5V_{rms}$ at a drive frequency of 300 kHz. A silicon tip coated with Pt was employed.

The spring constant of the cantilever was 5N/m associated with a free resonance frequency of 80 kHz.

Results and discussion

Thermal analyses

Thermal analysis was carried out to confirm the BCZT phase formation, by subjecting the BCZT-OX precursor to TG-DTA. The characteristic traces of BCZT-OX precursor are depicted in Fig. 2. These are distinctly different from that of individual oxalates.[18, 20] There are three major steps involved during the decomposition process of the precursor.

$$Ba_{0.85}Ca_{0.15}Ti_{0.9}Zr_{0.1}O(C_2O_4)_2.H_2O \xrightarrow{25-250^{\circ}C} Ba_{0.85}Ca_{0.15}Ti_{0.9}Zr_{0.1}O(C_2O_4).CO_3 + CO\uparrow + H_2O\uparrow \ (12\%)$$

$$Ba_{0.85}Ca_{0.15}Ti_{0.9}Zr_{0.1}O(C_2O_4).CO_3 \xrightarrow{250-675^{\circ}C} Ba_{0.85}Ca_{0.15}Ti_{0.9}Zr_{0.1}O_2CO_3 + CO\uparrow + CO_2\uparrow \ (21.2\%)$$

$$Ba_{0.85}Ca_{0.15}Ti_{0.9}Zr_{0.1}O_2.CO_3 \xrightarrow{675-800^{\circ}C} Ba_{0.85}Ca_{0.15}Ti_{0.9}Zr_{0.1}O_3 + CO_2\uparrow \ (16\%)$$

The total weight loss observed from TG is around 47.3%. While the theoretically calculated weight loss is ~ 49% (which is obtained by considering the total decomposition of $Ba_{0.85}Ca_{0.15}Zr_{0.1}Ti_{0.9}O.(C_2O_4)_2.H_2O$ precursor into $Ba_{0.85}Ca_{0.15}Zr_{0.1}Ti_{0.9}O_3$ phase). It is known in the literature that the possible decomposition reaction for oxalate complexes are: (i) dehydration, (ii) decomposition of the oxalate into a complex oxycarbonate and (iii) decomposition of the intermediate carbonate to phase pure compound.[14] The following steps are encountered in TG-DTA and explained as follows.

The first step (Endo I), in the temperature range of 25 - 250°C comprises the process of dehydration of water that takes place at 114°C followed by the release of carbon monoxide from the precursor that reflected as a small shoulder at 221°C. The

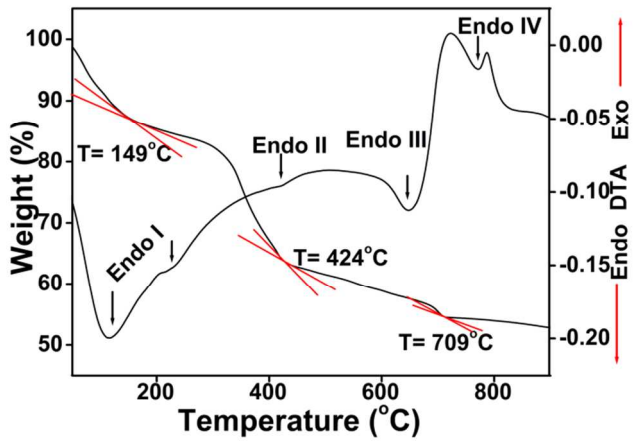

Fig.2 TG-DTA curves obtained in air ambience for BCZT-OX precursor powder (at the heating rate of 10°C/ min).

experimentally observed weight loss is 12.7% which is in reasonable agreement with that of calculated value of 12%. The residue at this step is $Ba_{0.85}Ca_{0.15}Zr_{0.1}Ti_{0.9}O(C_2O_4).CO_3$.The second step is associated with the thermal decomposition of oxalate (marked as Endo II & III) between 250 - 675°C, resulting in a release of carbon monoxide and carbon dioxide. The residue at this stage is $Ba_{0.85}Ca_{0.15}Zr_{0.1}Ti_{0.9}O_2.CO_3$. The experimentally observed weight loss associated with this step is around 22.6% which is comparable to the calculated value of 21.2%. The final decomposition step occurs in the 675 - 800°C temperature range with a release of carbon dioxide at 770°C (marked as Endo IV), giving rise to $Ba_{0.85}Ca_{0.15}Zr_{0.1}Ti_{0.9}O_3$. The observed weight loss for the final decomposition is 12% and the calculated value is around 16%. Based on the above observations, the following sequence of decomposition events are proposed for BCZT-OX complex precursor:

Infrared spectrum of the complex precursor

The formation of monophasic nature of BCZT is further confirmed by the FTIR analysis. Fig. 3(a-f) shows the FTIR spectra obtained for the as-prepared and the powder heat treated at various temperatures. The FTIR spectrum of precursor powder is distinctly different from that of final phase. The absorption bands that are observed in the 500–700cm^{-1} range are mainly attributed to the formation of metal oxide bonds (Ba-O, Ca-O, Zr-O and Ti-O bond).[21]

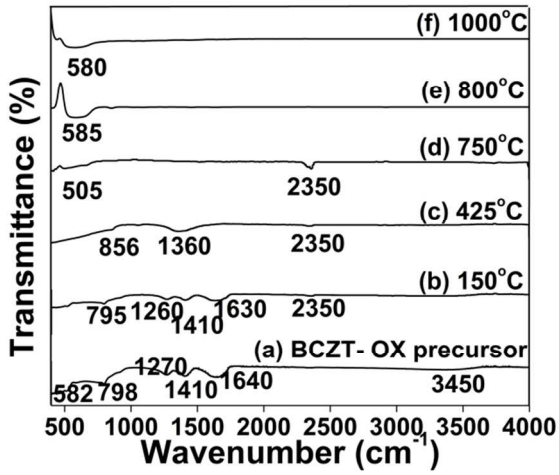

Fig.3 FTIR spectra of the precursor powder and the one heat treated at different temperatures.

The as-prepared powder exhibited absorption bands centered around 1270, 1410 and 1630 cm^{-1} which are attributed to the presence of oxalate anions with C_{2v} point group symmetry.[18] This oxalate anion facilitates the formation a bridging group between the metal atoms.[22] The band at 2350cm^{-1} is assigned to the asymmetric stretching mode of free carbon dioxide.[14] A strong absorption band witnessed at 3450 cm^{-1} is assigned to the asymmetric and symmetric OH stretching due to water adsorption

on the surface of powdered sample.[14] The bands with reduced intensity around 1260, 1410, 1630 and 2350 cm^{-1} are observed for the powder heat treated at 150°C. The disappearance of the band at 3450cm^{-1} confirms the process of dehydration taking place above 114°C. The sample that was heat treated at 425°C, exhibited bands around 1360 and 2350 cm^{-1}, indicating the presence of ν_{as} of the carbonate and asymmetric stretching mode of free carbon dioxide.[18] The obtained residue at 425° C was further heat treated above the third decomposition temperature (i.e. above 650°C) which exhibited the bands around 1420, 1590 and 2350 cm^{-1}. This confirms the prevalence of ionic carbonate (υ_{asy} at 1420 and 1590 cm^{-1}) and the band at 2350cm^{-1} confirms asymmetric stretching mode of free carbon dioxide. However, the samples subjected to heat treatment at 800° C and 1000° C did not exhibit any of these bands, confirming the decomposition of oxy carbonates into BCZT. The FTIR spectra recorded for this sample is very much consistent with the thermal analyses data and the decomposition mechanisms proposed.

X-ray structural characteristics

In order to study the effect of heat-treatment temperature on BCZT-OX precursor complex and to confirm the single phase formation of BCZT nanocrystalline powder, X-ray diffraction studies were performed on the samples heat treated at different temperatures (Fig. 4(a-g)). The patterns that are depicted in Fig. 4(a - c) suggest the presence of small fraction of residual amorphous phase besides a few low intensity Bragg peaks corresponding to BCZT phase.

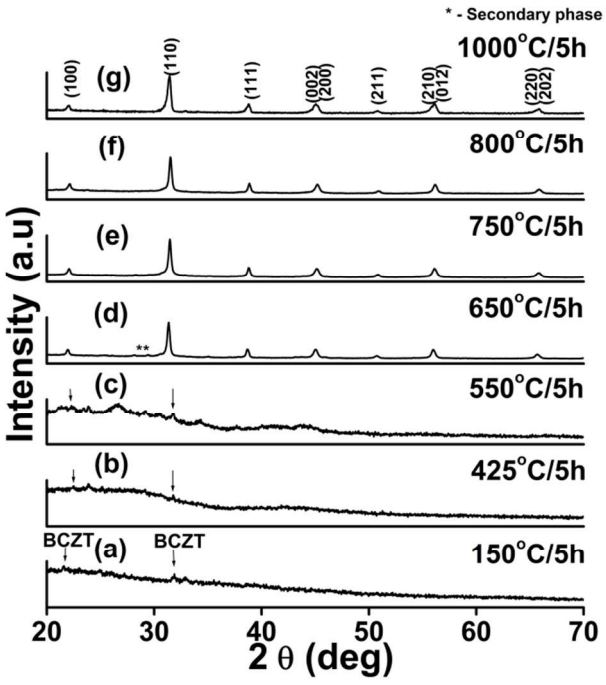

Fig.4 X-ray diffraction patterns recorded for the as-prepared powders heat treated at different temperatures (a) 150°C/5h (b) 425°C/5h, (c) 550°C/5h, (d) 650°C/5h, (e) 750°C/5h, (f) 800°C/5h and (g) 1000°C/5h

This establishes the onset of nucleation temperature of BCZT crystalline phase to be around 150°C. Similar observations were reported in the literature for $BaTiO_3$ compound.[14] The sample on further calcination at 650°C for 5h exhibited the Bragg peaks evidently corresponding to BCZT crystalline phase evolved in addition to the presence of less intensity precursor peaks suggesting that the decomposition process is still incomplete. However, the powder calcined at 750°C and above exhibited X-ray peaks that are identified with that of BCZT nanocrystalline phase.

In order to confirm the phase purity of the synthesized BCZT nanocrystalline powder, X-ray profile fitting refinements were carried out. It is known in the literature that $BaTiO_3$ powder heat treated in the 800-1000°C temperature range is likely to have both cubic and tetragonal phases.[23] So in order to assess the crystallographic phases associated with BCZT nanocrystalline powder, Profile refinements (LeBail fit) were carried out using Jana 2006 and profile parameters such as GU, GV, GW, LX and LY were refined using Pseudo-Voigt function. This technique has been employed to examine the phase purity as it is superior to that of a simple peak matching.[24] To begin with, the values of cell parameters and symmetry unrestricted angles of the cubic phase are given as input. The BCZT nanocrystalline powder refined with cubic phase did not show exact profile fit (Fig.5a). Subsequently, the cell parameters of tetragonal phase were given as inputs to the refined cubic phase of BCZT nanocrystalline powder. It showed an excellent fit and thus confirmed the coexistence of both cubic and tetragonal phases (Fig.5b). The volume fraction of tetragonal phase was obtained from refined cell parameters and found to increase slightly with the increase in heat treatment temperature. Table S1† shows the fitted profile parameters of BCZT nanocrystallites heat treated at 800° C and 1000° C/5h. Raman studies gave similar results that are discussed briefly in the next section. The following representations are used in the X-ray powder diffractograms; crosses for the observed pattern (Y_{obs}), green line for fitted profile, black line for the difference between observed and calculated profile ($Y_{obs.}$-Y_{calc}), tick marks are for reflection positions. The BCZT nanocrystalline powder refined with the cubic and tetragonal phases shows a good profile fit and the difference between the observed and calculated profile values ($Y_{obs} - Y_{calc}$) are negligible. The average crystallite size associated with the 800°C/5h heat treated powder was determined by considering the integrated width of the diffraction peak using the Scherrer equation:

$$t = \frac{0.9\lambda}{B\mathrm{Cos}\,\theta} \qquad (1)$$

Where, t is the crystallite size, λ is the wavelength of the radiation, θ is the diffraction angle and B is integrated full width at half maximum for a diffraction peak. Line broadening due to instrument was subtracted from the peak width before calculating the crystallite size using the following formula:

$$B^2 = B^2_{meas} - B^2_{equip} \qquad (2)$$

Where, B_{meas} = measured full width at half maximum for a peak, B_{equip}= instrumental broadening. To determine the instrumental

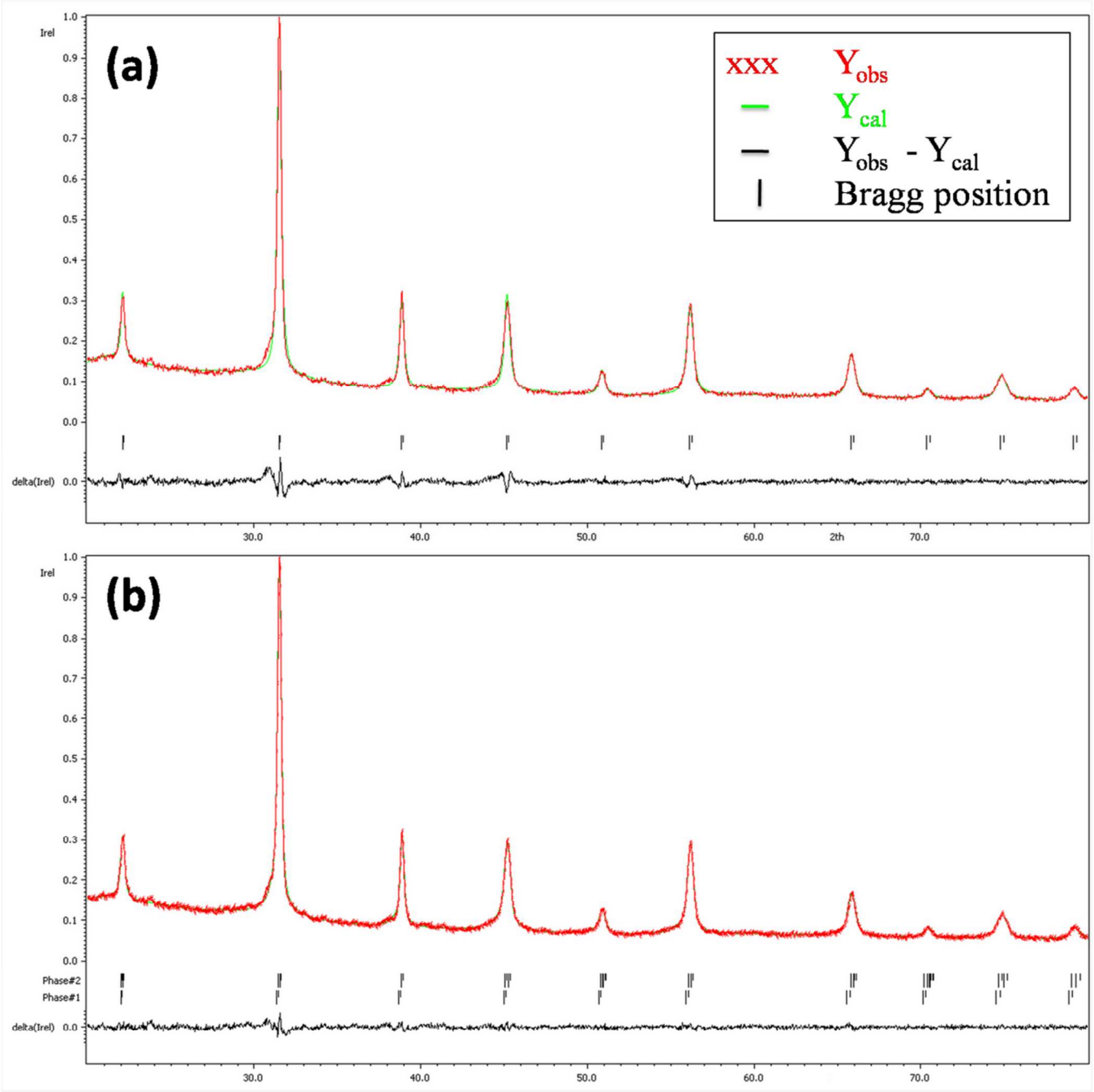

Fig.5 Fitted profile of BCZT nanocrystalline powder (a) with cubic phase and (b) cubic and tetragonal phases.

broadening, Si (silicon) standard (supplied along with the Pananalytical XRD instrument) was used. It was around B_{equip} = 0.131. The average crystallite size calculated using the diffraction peaks (100), (110), (111), (200) and (210) was around 20 - 50 nm for 800°C heat treated sample. These are consistent with that of TEM studies.

Raman studies

Raman spectra were recorded for the as-prepared and those powders heat treated at 800°C and 1000°C/5h. Raman study is more sensitive to the vibrational modes of the ferroelectric crystal systems, and thus confirms the formation of BCZT phase. [21, 25 - 28] The spectra recorded for all the three samples exhibited bands at 188, 298, 519 and 719 cm^{-1} corresponding to E_1 (TO_2) / $E_1(LO_1)$ / $A_1(LO_1)$, B_1/E (TO_3 + LO_2), $A_1(TO_3)$ and $A_1(LO_3)$/ E (LO_4) modes (Fig.6). The spectra obtained for the as-prepared powder showed weak vibrational modes with less intensity. The intensity of these peaks increased for the samples heat treated at higher temperatures. The peaks between 180 –300 cm^{-1} are assigned to asymmetric phonon vibrations of Ti-O bonds and those at 519 and 719 cm^{-1} are assigned to Ba - O bonds.[27] The peak at 519

cm^{-1} is common for both the cubic and tetragonal phases. [27] The peaks at 298 and 719 cm^{-1} confirm the presence of ferroelectric tetragonal phase of the sample. [27] The peak at 298 cm^{-1} appeared sharper for the powder heat treated at 1000°C than that of the as-prepared and the one heat treated at 800°C. These studies help

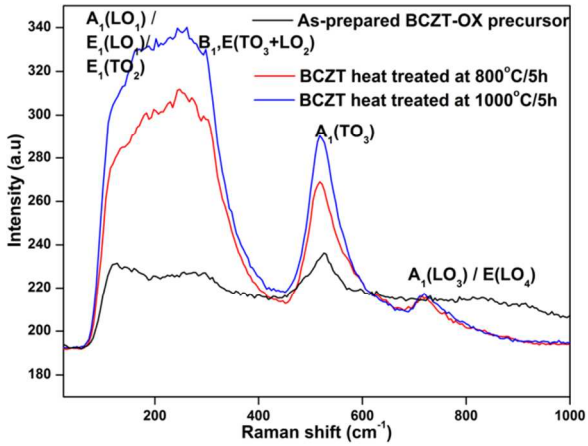

Fig.6 Room temperature Raman spectra for BCZT nanocrystalline powder

one to monitor the change in the volume fraction of the tetragonal phase with the increase in heat treatment temperature vis-à-vis crystallite size of the sample. There is a slight shift in the peak positions observed for the BCZT nanocrystalline powder compared to that of pure $BaTiO_3$ and is attributed to the crystallite size effect. These results evidently confirm the presence of local tetragonal phase associated with BCZT nanocrystalline powder.

Microstructural studies

Fig.7(a) shows the Transmission electron micrograph (TEM) obtained for BCZT nanocrystalline powder heat treated at 800°C/5h. It suggested the crystallite size to be below 50nm. Fig.7 (b & c) represents the SAED pattern and the high resolution lattice image recorded for the BCZT nanocrystallites. Interplanar spacing (d) calculated using the rings were 2.8 and 2.33 Å which correspond to (110) and (111) planes respectively. These values are in close agreement with those obtained by XRD studies. Fig. 7(d) depicts the Transmission electron micrograph obtained for BCZT powder heat treated at 1000°C/5h according to which the crystallite size has wide distribution and is in the 40 – 200nm range.

Interestingly, in the samples heat treated at 800°C and 1000°C/5h, the presence of ferroelectric domains are noticed using bright field image of TEM. The BCZT powder heat treated at 800°C/5h associated with crystallite size of around 20 – 50nm showed only a few domains (Fig. 8(a)). This is attributed to the predominance of cubic phase associated with these smaller crystallites. Whereas the one, heat treated at 1000°C/5h exhibited different domain patterns associated with high density that are depicted in Fig. 8 (b). The bright field images of BCZT powders heat treated at 800°C/5h and 1000°C/5h revealed the domain widths to be in the 0.9 – 1nm (Fig. 8(a)) and 3 - 4nm (Fig. 8(c)) respectively. Especially, in all these grains, simple lamellar-like domains (stripes) are clearly visible which indicate the presence of mostly 90° type ferroelectric domains lying on the {011} plane. The grain and nano domain size dependent piezoresponse are investigated and discussed in the latter part of this article.

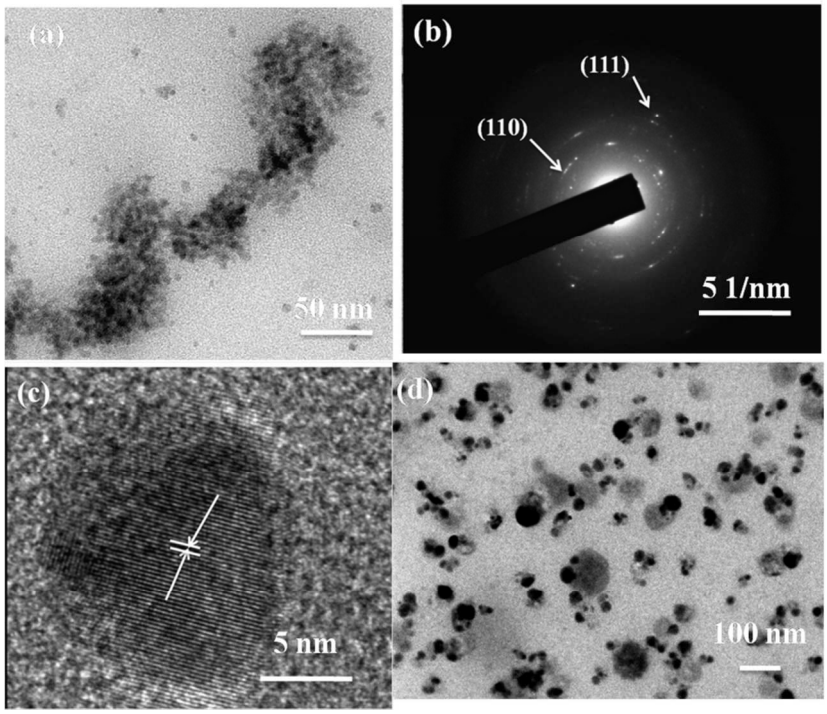

Fig.7 Transmission electron microscopy images for the BCZT nanocrystalline powder heat treated at 800°C/5h (a) bright field image, (b) SAED pattern, (c) HRTEM image and (d) bright field image for powder heat treated at 1000°C/5h.

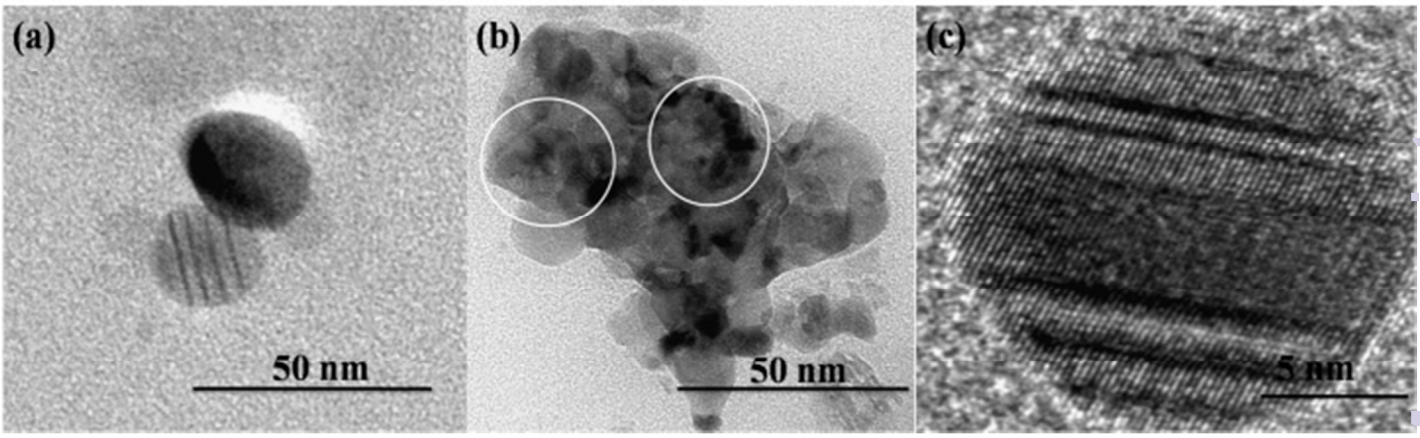

Fig.8 Bright field images showing ferroelectric domain patterns for the BCZT nanocrystalline powder heat treated at (a) 800°C/5h, (b) and (c) 1000 °C/5h.

Optical properties

The diffuse reflectance spectra were recorded (inset in Fig.9) in the wavelength range of 200 – 1000 nm for the samples heat treated at 800°C/5h (20 – 50nm) and 1000°C/5h (40 – 200nm). Kubelka Munk function[29] as given below was used to determine the optical bandgap of BCZT nanocrystallites.

$$F(R_\infty) = \frac{(1-R_\infty)^2}{2R_\infty} = \frac{K}{S} \qquad (3)$$

Where R_∞ is diffuse reflectance emanating from an infinitely thick sample and is related to the absorption coefficient (K) and scattering coefficient (S). Fig.9. shows the plot of $[F(R_\infty)h\upsilon]^{1/2}$ versus hυ from which the band gaps of BCZT nanocrystalline powders are evaluated by extrapolating the linear portions of the curves. The BCZT nanocrystalline powder having crystallites in the range of 20 – 50nm exhibited a band gap of 3.12 ± 0.02 eV where as the other sample in the present investigations has the band gap around 3.03 ± 0.02 eV. The value of band gap slightly increased with decrease in crystallite size which is attributed to the size effects. [30]

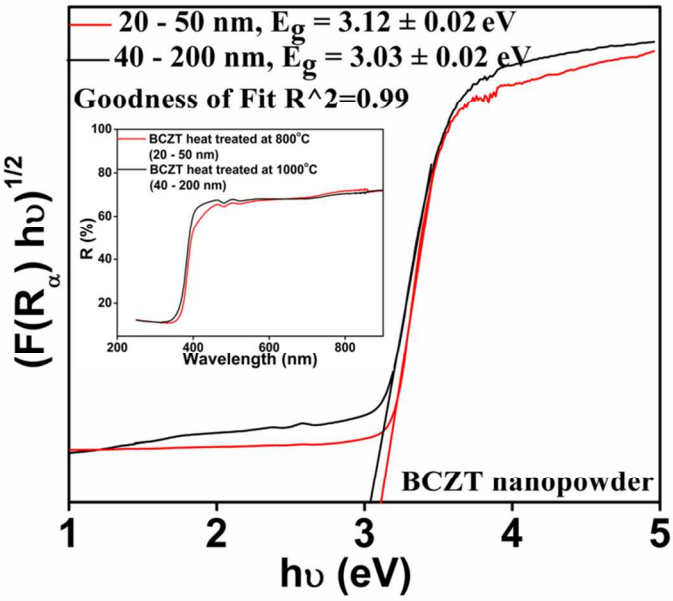

Fig.9 Plot of Kubelka–Munk function and the inset depicts diffuse reflectance spectra for the samples heat-treated at different temperatures.

Piezoelectric properties

The Piezoresponse of the BCZT nanocrystallites was studied using PFM method. Fig 10(a & b) and Fig. 10(c & d) shows the amplitude and phase response as a function of DC bias voltage. For this, drive amplitude of AC voltage of $5V_{rms}$ at a drive frequency of 300 kHz was applied between tip and the bottom electrode (conducting substrate). This causes the sample to vibrate at same frequency due to converse piezoelectric effect. [31] Therefore the resultant deformation of the sample was detected through vertical deflection of the cantilever interms of amplitude and phase as a function of bias voltage using a standard lock-in amplifier technique. [31] Fig. S1(a)† shows the topographical image of BCZT nanocrystallites heated at 1000°C/5h having maximum crystallite size of 70nm on the Pt substrate. Fig. S1(b&c)† shows the out of plane amplitude and phase image of the corresponding sample which showed better piezoelectric response than the other. Similar observation was made on the sample heat treated at 800°C/5h having crystallite size of 30nm. The bright area of the amplitude image clearly shows the piezo active area of the sample, whereas the contrast of bright and dark regions in the phase image depicts the polarization direction of the domains in the sample. [32] The bright regions indicate the positive domains (polarization pointing towards bottom electrode) and the dark regions depict the negative domains (polarization pointing towards top electrode). [32] The piezoelectric coefficient of the BCZT nanocrystallites was determined by positioning the tip across the bright area of the amplitude image which represents the piezo active area of the sample. Interestingly, the amplitude (pm) versus DC bias voltage (V) exhibited butterfly loops corresponding to displacement (pm) versus DC bias voltage which contains information about piezoelectric deformation

under an applied DC bias voltage[33] of the 30nm and 70nm sized BCZT crystallites which are depicted in Fig.10(a) and Fig.10(b) respectively. Phase (°) versus DC bias (V) plots which demonstrate the local polarization switching behavior[34] for 30nm and 70nm sized crystallites are depicted in Figs.10(c) and Fig.10(d) respectively. The phase difference characteristics for both 30nm and 70nm sized crystallites confirm 180° polarization switching under DC bias voltage which in turn establishes the presence of 180° domains in these nanocrystallites.[7, 35] From the above curve Fig.10 (a) and Fig.10 (b), the value of local d_{33} coefficient of 30 nm and 70 nm sized crystallite was estimated through the following equation

$$(V - V_I)\, d_{33} = (D - D_I) \qquad (4)$$

where D is the measured value of piezoelectric deformation, V is the applied voltage, D_I and V_I is the piezoelectric deformation and applied voltage of the intersection. [33] Figs.10 (e) and 10(f) depicts the piezoresponse (d_{33}) curve as a function of DC bias voltage for both 30nm and 70nm sized BCZT crystallites. The 30nm sized BCZT crystallite exhibited piezoelectric coefficient (d_{33}) of 4 pm/V at the maximum voltage of 8V. The coercive voltage (0.54V) was evaluated using the equation $(V_c^+ - V_c^-)/2$ where V_c^+ and V_c^- are forward and reverse coercive bias voltages. [36]

Interestingly the piezoelectric coefficient (d_{33}) obtained for 70nm sized BCZT crystallite is 47pm/V at the maximum voltage of 5V. The coercive voltage is 0.33V which is quite low as compared to that of the other samples in the present study. In order to compare with coercive voltage of the bulk BCZT ceramic, the above sample was sintered at 1300°C and obtained crystallite size of 7µm. The polarization versus electric field (P-E) loop that was recorded for these samples is shown in Fig. S2†. It is well known in the literature that the domain size has a strong dependence on crystallite size.[37 - 39] The low piezoelectric coefficient coupled with high coercive voltage (0.54V) that is encountered for 30 nm sized crystallite is ascribed to the lack of well defined domain walls as these were expected to play crucial role in the piezoelectric characteristics of the samples. These results suggest that though the crystallites at the nanoscale exhibit piezoelectric phenomenon, one has to have large enough (>50nm) size to visualize reasonably good piezoelectric properties. Indeed the value obtained for 70nm sized crystallite is twice that of $BaTiO_3$ nanocrystallites (20pm/V). [28, 40- 43]

Conclusions

The BCZT nanocrystalline powder derived from oxalate precursor showed the coexistence of both cubic and tetragonal phases as confirmed by XRD data followed by profile fitting and Raman studies. Transmission electron microscopy carried out on the samples heat treated at 800°C/5h and 1000°C/5h revealed lamellar type domain patterns with varying domain width. These nanocrystallite size dependent piezoresponse studies suggest that ≈70nm sized crystallites of BCZT may be of potential use for miniaturized piezoelectric/ferroelectric based device applications.

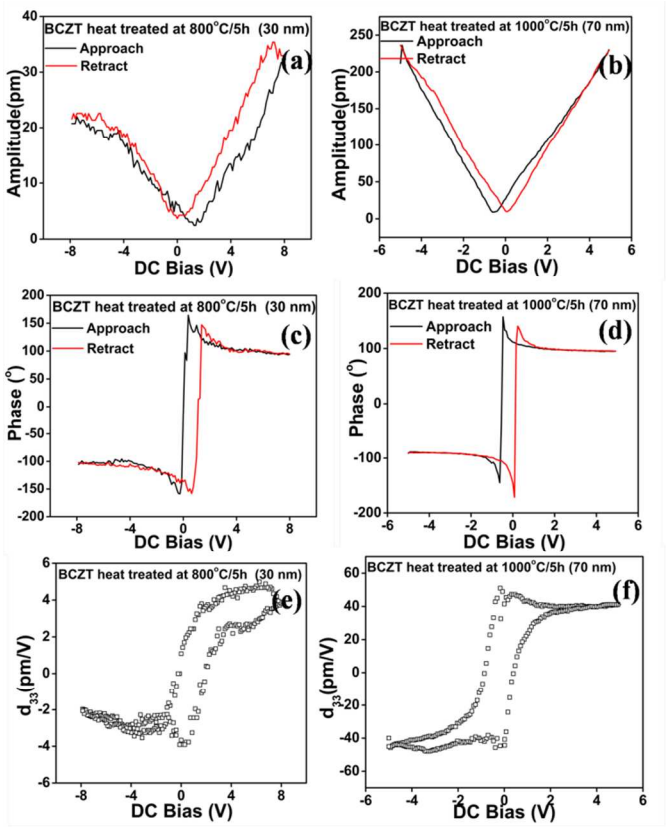

Fig.10 (a & b) Amplitude, (c & d) Phase and (e & f) Piezoresponse (d_{33}) versus DC bias voltage of BCZT nanocrystalline powder.

References

1 Pil Gu Kang, Byung Kil Yun, Kil Dong Sung, Tae Kwon Lee, Minbaek Lee, Nuri Lee, Seol Hee Oh, William Jo, Hae Jin Seog, Chang Won Ahn, Ill Won Kim and Jong Hoon Jung, *RSC Adv.,* 2014, **4**, 29799.

2 Kwi-Il Park , Minbaek Lee , Ying Liu , San Moon , Geon-Tae Hwang , Guang Zhu , Ji Eun Kim , Sang Ouk Kim , Do Kyung Kim , Zhong Lin Wang , and Keon Jae Lee, *Adv. Mater.,* 2012, **24**, 2999.

3 Jong Hoon Jung, Chih-Yen Chen, Byung Kil Yun, Nuri Lee, Yusheng Zhou, William Jo, Li-Jen Chou and Zhong Lin Wang, *Nanotechnology*,2012, **23**, 375401.

4 Jong Hoon Jung, Minbaek Lee, Jung-Il Hong, Yong Ding, Chih-Yen Chen, Li-Jen Chou, and Zhong Lin Wang, *ACS Nano*, 2011, **5**, 10041.

5 K. Momeni, G. M. Odegard, and R. S. Yassar, *J. Appl. Phys.,*2010, **108**, 114303.

6 Shiyou Xu, Yao-wen Yeh, Gerald Poirier, Michael C. McAlpine, Richard A. Register, and Nan Yao, *Nano Lett.*, 2013, **13**, 2393.

7 Han Byul Kang, Jiyoung Chang, Kisik Koh, Liwei Lin, and Yong Soo Cho, *ACS Appl. Mater. Interfaces,* 2014, **6**, 10576.

8 Byung Kil Yun, Yong Keun Park, Minbaek Lee, Nuri Lee, William Jo, Seongsu Lee and Jong Hoon Jung, *Nanoscale Res. Lett.,* 2014, **9**,4.

9 J. Rodel, W. Jo, K. T. P. Seifert, E. M. Anton, T. Granzow, and D. Damjanovic, *J. Am. Ceram. Soc.,* 2009, **92**, 1153.

10 W. Liu and X. Ren, *Phys. Rev. Lett,.* 2009, **103**, 257602.

11 P. Wang, Y. Li, and Y. Lu, *J. Eur. Ceram. Soc.,* 2011, **31**, 2005.
12 J. Wu, D. Xiao, W. Wu, J. Zhu, and J. Wang, *J. Alloys Compd.,* 2011, **509**, L359.
13 S. Ye, J. Fuh, L. Lu, Y.-L. Chang, and J.R.Yang, *RSC Adv.,* 2013, **3**, 20693.
14 H.S.Gopalakrishnamurthy, M. Subba Rao and T.R. Narayanan Kutty, *J. inorg, nucl Chem.,* 1975, **37**, 891.
15 Sven van der Gijp, Louis Winnubst and Henk Verweij, *J. Mater. Chem.,* 1998, **8**, 1251.
16 S. Otta and S. D. Bhattamisra, *J. Therm. Anal.,* 1994, **41**, 419.
17 Anand Kumar Sharma and N.K. Kaushik, *Thermochim. Acta,* 1985, **83**, 347.
18 P. Thomas, K. Dwarakanath, K.B.R. Varma, and T.R.N. Kutty, *J. Phys. Chem. Solids*, 2008, **69**, 2594.
19 P. Bharathi and K. B. R. Varma, *J. Appl. Phys.,*2014, **116**, 164107.
20 F. G. R. Gimblett, A. Hussain and K. S. W. Sing, *J. Therm. Anal.,*1988, **34**, 1001.
21 Zeng-mei Wang, Kuan Zhao, Xin-li Guo, Wei Sun, Hua-long Jiang, Xue-qin Han, Xu-tang Tao, Zhen-xiang Cheng, Hong-yang Zhao, Hideo Kimura, Guo-liang Yuan, Jiang Yin and Zhi-guo Liu, *J. Mater. Chem. C.,* 2013, **1**, 522.
22 K. Nakamoto, Infrared and Raman Spectra of Inorganic and Coordination Compounds, third ed., Wiley, New York, 1978 part III, p. 233–237.
23 E. K. Akdogan, M. R. Leonard, and A. Safari, Handbook of Low and High Dielectric Constant Materials and Their Applications (Academic Press, USA, 1999),p.61.
24 V. Petricek, M. Dusek and L. Palatinus, Jana 2000, 08/11/2007 ed., 2007.
25 Venkata Sreenivas Puli, Ashok Kumar, Douglas B Chrisey, M Tomozawa, J F Scott and Ram S Katiyar, *J. Phys. D: Appl. Phys.,* 2011, **44,** 395403.
26 U. M. Pasha, H. Zheng, O. P. Thakur, A. Feteira, K. R. Whittle, D. C. Sinclair, and I. M. Reaney, *Appl. Phys. Lett.,*2007, **91**, 062908.
27 Venkata Ramana E., A. Mahajan, M.P.F. Graca, S.K. Mendiratta, J.M. Monteiro, M.A. Valente, *Mater. Res. Bull.,* 2013, **48**, 4395.
28 Xiangyun Deng, Xiaohui Wang, Hai Wen, Aiguo Kang, Zhilun Gui, and Longtu Li, *J. Am. Ceram. Soc.,* 2006, **89**, 1059.
29 P. Kubelka, *J. Opt. Soc. Am.,* 1948, **38**, 448.
30 Keigo Suzuki and Kazunori Kijima, *Jpn. J. Appl. Phys.,* 2005, **44,** 2081.
31 A Gruverman and A Kholkin, *Rep. Prog. Phys.,* 2006, **69,** 2443.
32 A. L. Kholkin, I. K. Bdikin, D. A. Kiselev, V. V. Shvartsman and S.H. Kim, *J Electroceram*, 2007, **19,** 81.
33 Z. Chen, J. Huang,Y. Yang, Y. Wang, Y. Wu, H. He, X. Wei, Z. Ye, H. Zeng, H. Cong and Z. Jiang, *RSC Adv.,* 2012, **2**, 7380.
34 A.L. Kholkin, S. V. Kalinin, A. Roelofs and A. Gruverman, Review of Ferroelectric Domain Imaging by Piezoresponse Force Microscopy, Alexei Gruverman Publications, 2007, p. 46.
35 Debasish Mohanty, Girija S. Chaubey, Amin Yourdkhani, Shiva Adireddy, Gabriel Caruntu and John B. Wiley, *RSC Adv*., 2012, **2**, 1913.
36 H. B. Kang, J. Chang, K. Koh, L. Lin, and Y. S. Cho, *ACS Appl. Mater. Interfaces* 2014, **6**, 10576.
37 S. B. Ren, C. J. Lu, J. S. Liu, H. M. Shen, and Y. N. Wang, *Phys. Rev. B*, 1996, **54**,14337.
38 Huizhong Zeng, Shengbo Lu, Linshan Dai, Jingsong Liu, Zhihong Wang, Changming Zuo, *Mater. Lett.,* 2005, **59**, 2808.
39 A Roelofs, T Schneller, K Szot and R Waser, *Nanotechnology*, 2003, **14**, 250,
40 Xiangyun Deng, Xiaohui Wang, Hai Wen, Liangliang Chen, Lei Chen, and Longtu Li, *Appl. Phys. Lett.,*2006, **88**, 252905.
41 Xiaohui Wang, Xiangyun Deng, Hai Wen, and Longtu Li, *Appl. Phys. Lett.,* 2006, **89**, 162902.
42 Maria Teresa Buscaglia, Vincenzo Buscaglia, Massimo Viviani, Jan Petzelt, Maxim Savinov, Liliana Mitoseriu, Andrea Testino, Paolo Nanni, Catalin Harnagea, ZheZhao and Mats Nygren, *Nanotechnology,* 2004, **15**, 1113.
43 Yongyong Zhuang, Fei Li, Guang Yang, Zhuo Xu, Jinglei Li, Bi Fu, Yaodong Yang, and Shujun Zhang, *J. Am. Ceram. Soc.,* 2014, **97**, 2725.

Graphical Abstract:

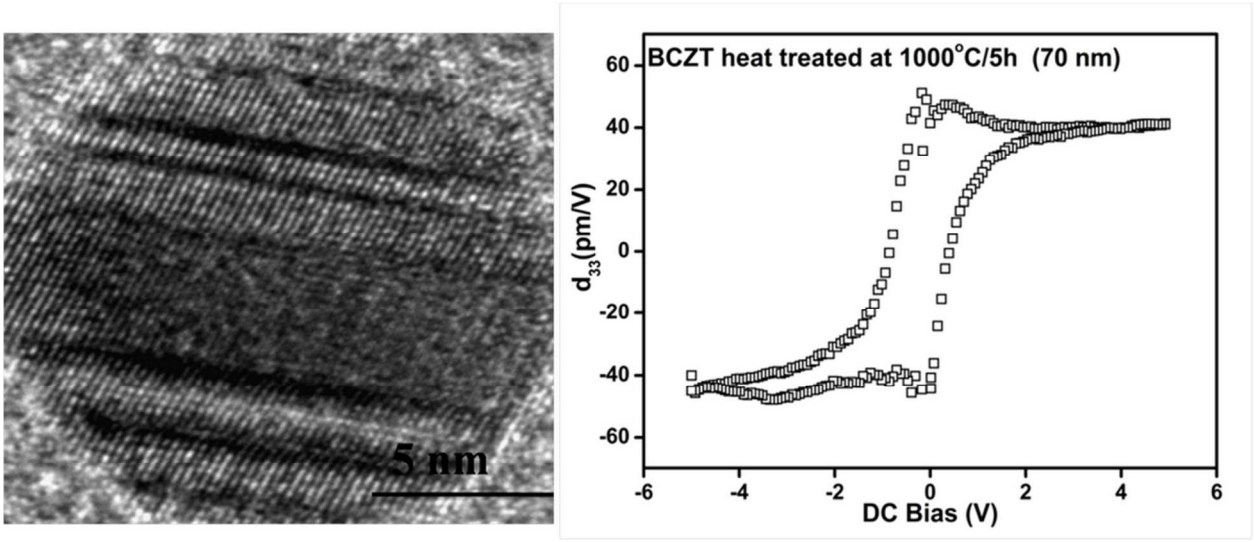

Ferroelectric domain pattern and Piezoresponse (d_{33}) versus DC bias voltage for the BCZT nanocrystalline powder.